Glycopolymeric Micellar Nanoparticles for Platelet-Mediated Tumor-Targeted Delivery of Docetaxel for Cancer Therapy

Yan Zhang, Yi Li, Jieyu Gu, Jun Wu, Yongxin Ma, Guodong Lu, Mihail Barboiu, Jinghua Chen

Glycopolymeric Micellar Nanoparticles for Platelet-mediated Tumor-targeted Delivery of Docetaxel for Cancer Therapy

Yan Zhang,[,$] Yi Li,[$] Jieyu Gu,[$] Jun Wu,[$] Yongxin Ma,[$] Guodong Lu,[$] Mihail Barboiu,*[,#] Jinghua Chen*[,$]

[$]Key Laboratory of Carbohydrate Chemistry and Biotechnology, Ministry of Education, School of Life Sciences and Health Engineering, Jiangnan University, Wuxi, 214122, P.R. China.

[#]Institut Europeen des Membranes, Adaptive Supramolecular Nanosystems Group, University of Montpellier, ENSCM-CNRS, UMR5635, Place E. Bataillon CC047, 34095 Montpellier, France

KEYWORDS: Glycopolymer, Platelets, Drug delivery, Nanoparticles, Cancer therapy

ABSTRACT: The high accumulation of therapeutic agents in tumors is crucial for cancer treatment. Compared to the passive tumor-targeting effect, active tumor-targeting delivery systems, primarily mediated by peptides with high production costs and reduced circulation time, are highly desired. Platelets-driven technologies have opened new avenues for targeted drug delivery prevalently through membrane coating strategy that involves intricate manufacturing

procedures or the fucoidan-mediated hitchhiking method with limited platelet affinity. Here, a novel type of amphiphilic glycopolymer self-assembled micellar nanoparticles has been developed to adhere on the natural activated platelets in blood. The simultaneous integration of fucose and sialic acid segments into the glycopolymers enables closer mimicry of the structure of P-selectin glycoprotein ligand-1 (PSGL-1), thereby increasing the affinity for activated platelets. It is resulting in the formation of Glycopolymeric-micelles-platelets hybrids, facilitating targeted drug delivery to tumors. The selective platelets-assisted cellular uptake of docetaxel (DTX)-loaded glycopolymeric micelles, lead to lower IC_{50} values against 4T1 cells than that of free DTX. The directed tumor-targeting effect of activated platelets has significantly improved the tumor accumulation capacity of the glycopolymeric nanoparticles, with up to 21.0% found in tumors within the initial 0.2 h. Additionally, with acid-responsive drug release and inherent anti-metastasis properties, the glycopolymeric nanoparticles ensured potent therapeutic efficacy, prolonged survival time and reduced cardiotoxicity, presenting a new and unexplored strategy for platelet-directed drug delivery to tumors, showing promising prospects in treating localized tumors and preventing tumor metastasis.

INTRODUCTION

Cancer has long been a serious threat to human health. With the fast advances in anti-tumor drug discovery, researchers have come to realize the crucial importance of therapeutic agent accumulation in tumors for cancer chemotherapy. Traditional passive tumor-targeting, directed by the enhanced permeability and retention (EPR) effect of nanocarriers, results in only 0.7% of injection dose (median) reaching solid tumors.[1-2] Various active tumor-targeting strategies have been developed, primarily mediated by antibodies, peptides, or aptamers, such as the classical Arg-Gly-Asp (RGD) that binds to αvβ3 integrin.[3] However, these targeting moieties are often accompanied by high production cost and reduced circulation half-life.[4] Natural polysaccharides, such as hyaluronic acid and fucoidan, have also demonstrated targeting effects on tumors, but with significantly lower binding affinity.[5] Meanwhile, the extracting and the purification of polysaccharides from natural sources is a laborious process, often leading to complex compositions and heterogeneous activities.[6-7] In this regard, synthetic glycopolymers with customizable oligo- or mono-saccharides grafted as side chains, possessing straightforward synthetic method and structures,[8-10] can mimic the structures and functions of natural polysaccharides,[11-15] but is rarely used as anchoring moieties for active tumor-targeted drug delivery.

Among the emerging biomimetic vesicles with active tumor-targeting effect, platelets, an essential blood component, can be activated and recruited back to the tumor site, playing a critical role in multiple stages of tumor cell growth and metastasis.[16-18] By leveraging its tumor-homing property,[19-23] strategies involving platelet membrane separation and surface engineering have been developed to enhance targeting efficiency and improve treatments for multiple myeloma, thrombus, etc.[24-27] Meanwhile, intricately designed drug-loaded nanoparticles with a

strong affinity for activated platelets have been applied for the targeted treatment of tumors, thrombolysis, and cardiovascular diseases.[28-30] These nanoparticles can bind the accessible receptors on platelets, such as GPIIb/IIIa, GPIb-V-IX and P-selectin.[31] For example, fucoidan has been reported with the ability to bind P-selectin,[32-33] but with substantially lower efficiency than sialyl-Lewis X (sLeX) found in P-selectin glycoprotein ligand-1 (PSGL-1).[34] Considering the structure of sialylated fucosylated tetrasaccharide of sLeX, we have previously reported a series of glycopolymers with the hybrid incorporation of sialic acid, fucoses and heparin disaccharides to mimic the structure of PSGL-1, leading to significantly reduced adhesion between activated platelets and B16 cells, as well as excellent anti-tumor metastasis activity.[35] This finding prompted us to further explore the potential application of these activated platelets-adhesion glycopolymers for tumor-targeted drug delivery and subsequent therapy.

Herein, *denovo* designed glycopolymer-based nanoparticles with platelet-adhesion ability are used for the targeted delivery of docetaxel (DTX) to tumors. The amphiphilic glycopolymers are synthesized by copolymerizing hydrophilic fucose/sialic acid segments with a hydrophobic dodecylamine component,[36] resulting in the formation nano-sized micelles *via* self-assembly in water (Figure 1). Due to the critical roles of synergistic fucosylation and sialylation in the functions of PSGL-1,[37-38] the simultaneous integration of fucose and sialic acid into the glycopolymers provides significantly enhanced multivalent affinity towards activated platelets that can actively guide the adhered glycopolymeric nanoparticles to tumor sites through their tumor-homing property. Furthermore, the pH-responsive breakdown of acylhydrazone bonds in the glycopolymer micelles enables targeted drug release in the acidic tumor environment.[39-40] The considerably strengthened tumor-targeting and retention properties, along with the

responsive drug release and inherent anti-metastasis abilities of the glycopolymeric nanoparticles, can greatly contribute to highly efficient cancer therapy of the next generations.

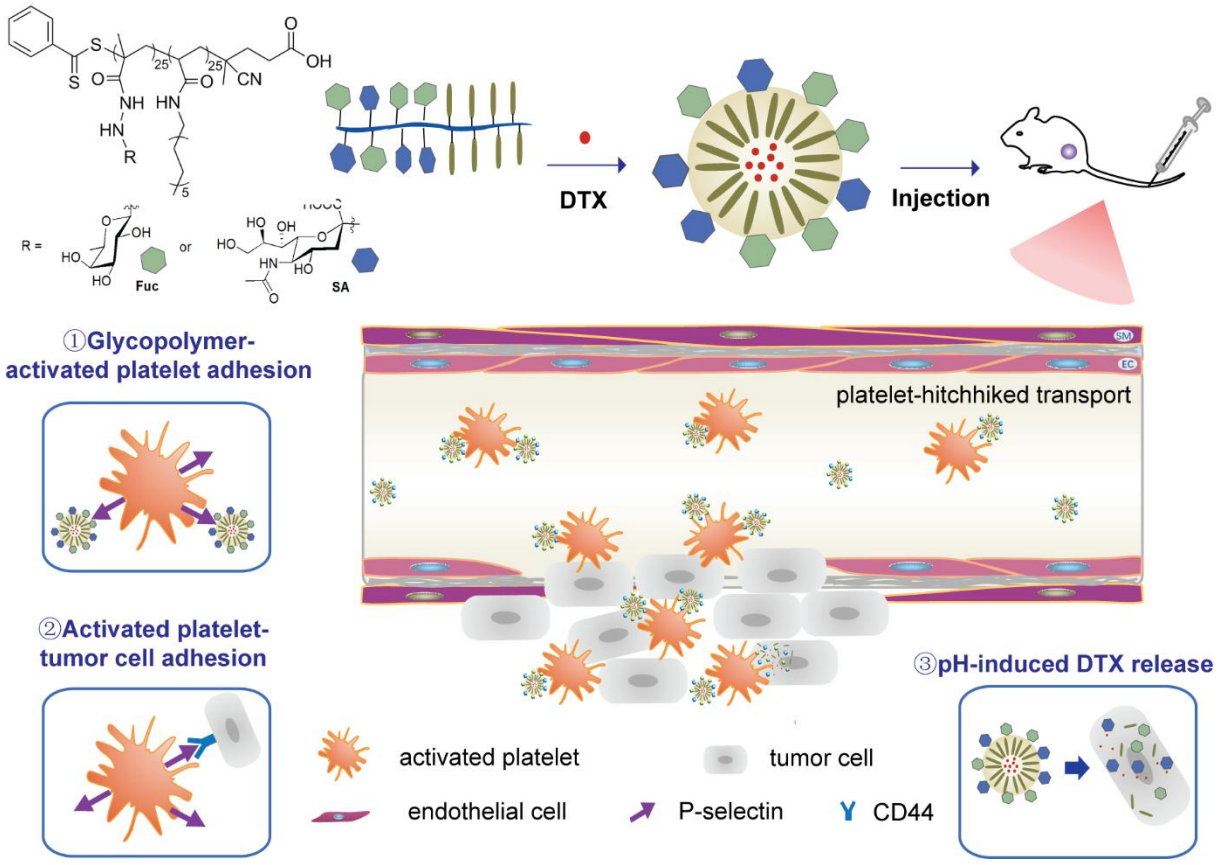

Figure 1. Schematic illustration of the preparation of DTX loaded (red dots)-fucose (Fuc, green), sialic acid (SA, blue), and dodecylamine (khaki) amphiphilic glycopolymeric nanoparticles and their platelet-mediated tumor-targeting and anti-tumor metastasis properties.

RESULTS AND DISCUSSION

Syntheses and characterization of the amphiphilic glycopolymeric nanoparticles. To construct nano-sized micelles for drug delivery, glycopolymers were designed with the synergistic incorporation of both saccharide-based hydrophilic segments and the dodecylamine-based hydrophobic fragments.[9] Initially, the polymerizable monomers were synthesized by connecting methacryloyl hydrazide or acrylic acid onto fucose/sialic acid structure or dodecylamine (Scheme S1-S3), respectively. Subsequently, the glycopolymers were synthesized

straightforwardly from a stepwise reversible addition-fragmentation chain transfer (RAFT) process (Scheme S4),[41-42] and their structure was confirmed by ^{1}H NMR (Figure S1-S5) and FT-IR spectroscopies (Figure S6). Additionally, their molecular weights were determined to be between 15-28 kDa (Table S1, Figure S7) by gel permeation chromatography (GPC). The nano-sized micelles were then prepared by self-assembly in water. Dynamic light scattering (DLS) analysis revealed that the particle sizes for nanoparticles of homoglycopolymers **P-Fuc** (100%Fuc), **P-SA (**100% SA) and of heteroglycopolymer **P-SF** ([SA]/[Fuc] = 1:1) were 90.7, 137.5, and 113.6 nm, respectively (Table S2, Figure 2A), consistent with their morphological profiles (Figure 2B) observed though transmission electron microscopy (TEM). The relatively smaller size of **P-Fuc** can be attributed to the lower molecular weight of the **Fuc**-grafted glycopolymer. In addition, nanopartielce **P-Fuc** demonstrated good micellar stability for a 7 d observation period at r.t. (Figure S8). Importantly, all the glycopolymers exhibited excellent cyto- and hemo-compatibility in MTT and hemolysis assays (Figure 2C-D), demonstrating great potential for any further biological applications.

The anti-tumor drug DTX was next loaded into the obtained nanoparticles using the solvent evaporation method. After DTX encapsulation, the particle sizes of all samples significantly increased but still maintained around 120-130 nm, with PDI values around 0.2, indicating uniform diameters of the newly generated spheres. The encapsulation efficiency (EE) and drug loading (LC) were calculated and summarized in Table S2. For glycopolymers **P-Fuc**, **P-SA** and **P-SF**, the calculated EE value were 66.4%, 63.8% and 73.3% respectively; the LC values were measured at 16.6%, 15.9% and 19.3%, respectively, with slightly higher values for glycopolymer **P-SF**. The acylhydrazone bonds embedded in the glycopolymers inherited pH-responsiveness, causing bond breakage and hastening drug release in an acidic environment. As shown in Figure

2E, all the glycopolymeric nanoparticles exhibited slow drug release rate at the physiological pH of 7.4, with 20% release in the first 8 h and 30% overall in 56 h. Meanwhile, much faster DTX release rates were observed at the endosomal pH of 5.5,[43-45] with the highest DTX release profile (69% in 56 h) found for nanoparticle **P-SF**/DTX. This pH-responsive drug release property can be highly beneficial for the DOX accumulation inside the acidic tumor environment.

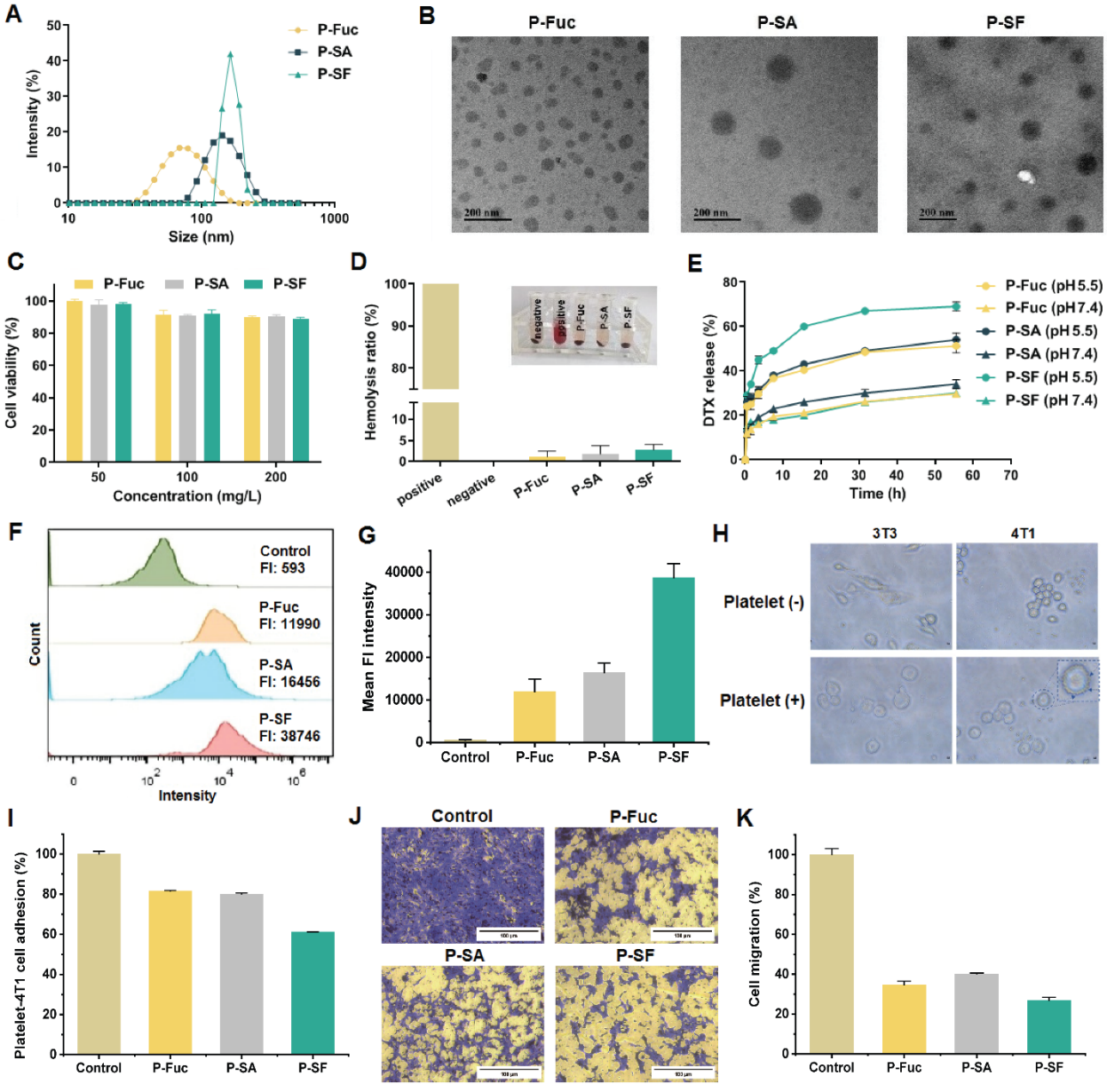

Figure 2. Glycopolymer-amphiphilic nanoparticles: (A) DLS size distribution and (B) TEM images of homo-glycopolymer **P-Fuc**; **P-SA** and hetero-glycopolymer **P-SF** ([SA]/[Fuc] = 1:1).

(C) MTT assay after incubation for 24 h and (D) hemolysis test of the glycopolymeric nanoparticles. (E) In vitro release of drug-loaded nanoparticles. Data are presented as mean ± SD (n=5). Adhesion of glycopolymeric nanoparticles to platelets tested by (F-G) flow cytometry and the quantified mean FI intensities. (H) Adhesion of platelets to 3T3 and 4T1. Scale bar =10 μm. (I) The impacts of glycopolymers on the adhesion between activated platelets and 4T1 cells. (J-K) Transwell assay of 4T1 cells migration with the presence of glycopolymeric nanoparticles.

Platelet-facilitated tumor-targeting effect. Glycopolymers with grafted fucose **P-Fuc** and sialic acid **P-SA** segments were designed to mimic the structure of PSGL-1, which triggers P-selectin mediated binding to the activated platelets and subsequent tumor-homing effect.[35] Thus, the binding ability of the rhodamine B-tagged glycopolymers with activated platelets was first evaluated by confocal laser scanning microscopy. As a result, compared to homoglycopolymers **P-Fuc** and **P-SA**, a significantly larger number of heteroglycopolymer **P-SF** were observed adhering to the platelet-covered plates (Figure S9). Additionally, quantitative analysis by flow cytometry revealed a similar pattern, with glycopolymer **P-SF** displaying the highest fluorescence intensity, more than twice that of monofunctional glycopolymers **P-Fuc** or **P-SA** (Figure 2F-G). This phenomenon can be explained by the synergetic presence of **Fuc** and **SA** segments in glycopolymer **P-SF**, better mimicking the structure of PSGL-1 and resulting in stronger multivalent synergetic interactions with activated platelets.

The adhesion of tumor cells to activated platelets is known as an essential step in tumor hematogenous metastasis.[46] To verify this adhesion and the tumor-homing effect of activated platelets in vitro, the activated or unactivated platelets were co-incubated with normal cells (3T3) or tumor cells (4T1), respectively. As shown in Figure 2H, only activated platelets were observed as small spherical bulges on the surfaces of 4T1 cells, indicating strong adhesion to tumor cells. Furthermore, in the presence of different glcopolymers, the binding between activated platelets and 4T1 cells has been weakened to some extent; for instance, a 39% decrease in adhesion was observed with glycopolymer **P-SF** (Figure 2I, Figure S10). Since there are

several receptors on tumor surfaces that can bind to P-selectin, such as PSGL-1, CD44 and CD24, the presence of PSGL-1 mimetic glycopolymers only partially hindered the recognition between activated platelets and tumor cells. However, this adhesion impacts of the glycopolymers still significantly inhibits 4T1 cell migration, where 65%, 60% and 73% of the cell population in the **P-Fuc**, **P-SA** and **P-SF** groups, respectively, were prevented from migration in the Transwell assay (Figure 2J-K). Moreover, the adhesion experiment between rhodamine B-tagged glycopolymer **P-SF** to platelets from tumor carrying mice has established the "activated" character of the circulating platelets from tumor-bearing animals (Figure S11). These studies confirmed the successive tumor-targeting effects of the glycopolymers, mediated by the P-selectin on the surface of activated platelets, while revealing the inherent anti-metastasis ability of the glycopolymers.

Enhanced and selective cellular uptake. High cellular uptake is a prerequisite for efficient drug delivery and the studied glycopolymer-platelet complex can accelerate this process by mediating tumor cell adhesion. Thus, the glycopolymeric nanoparticles were tagged with rhodamine B for cellular uptake assays on 4T1 cells. As shown in Figure 3A and the semi-quantification analysis in Figure S12a, all the glycopolymeric nanoparticles showed good cell penetration after 4 h, while **P-SF** demonstrated a significantly faster rate of cellular uptake compared to **P-Fuc** and **P-SA**, with fluorescent intensity detected inside the cells after 15 min of incubation. Additionally, Rhodamine B-tagged DTX showed slower endocytosis rates upon delivery of the nanoparticles (Figure S13) than the glycopolymers alone, while **P-SF**/DTX still showed a stronger fluorescent intensity than other DTX-loaded nanoparticles within the same timeframe. This trend was consistent with their binding ability to activated platelets, indicating critical role of the platelet-mediated tumor recognition.

Since the activated platelet is crucial for glycopolymer adhesion and tumor-targeting, the impacts of its presence on cellular uptake of the nanoparticles were next examined. 4T1 cells were pre-incubated with activated platelets for 30 min, followed by continuous incubation with nanoparticles **P-Fuc**, **P-SA** and **P-SF** for 2 h. As shown in Figure 3B and the semi-quantification analysis in Figure S12b, pre-incubation with activated platelets clearly improved the cellular uptake of all the nanoparticles. This improvement can be attributed to "bridging" mediating function of nanoparticle activated platelets, which closely connected the glycopolymers and the tumor cells, thereby promoting cellular uptake. In contrast, NIH 3T3 cells, representing normal cells, exhibited minimal cellular uptake of **P-Fuc**, **P-SA** or **P-SF** after 2 h of incubation, regardless of the presence of activated or unactivated platelets, indicating the high selectivity of these glycopolymeric nanoparticles for tumor cells.

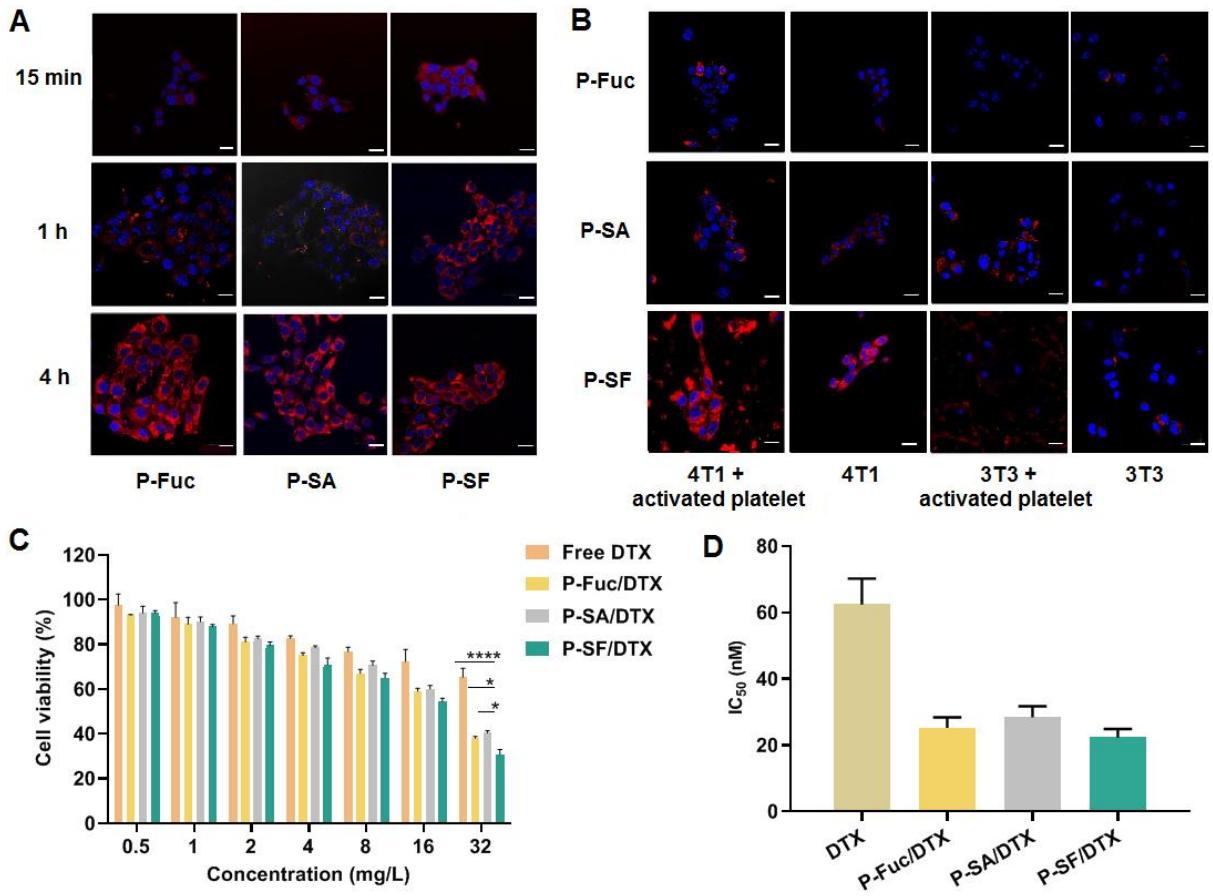

Figure 3. Cellular uptake of glycopolymers (A) incubated with 4T1 cells for 15 min, 1 h and 4 h. Red: glycopolymer-rhodamine B; blue: DAPI for staining cell nucleus. Scale bar =20 μm; (B) incubate with 4T1 and 3T3 cells for 2 h with or without activated platelet. Red: rhodamine B-tagged glycopolymers; blue: DAPI for staining cell nucleus. Scale bar =20 μm. (C) Cell viability after incubating with DTX, **P-Fuc**/DTX, **P-SA**/DTX, **P-SF**/DTX, respectively, for 24 h. Data are presented as mean ±SD (n =6, * $p < 0.05$, **** $p < 0.0001$). (D) Calculated IC_{50} values of the DTX-loaded glycopolymers.

In Vitro Anti-tumor Activity of the Nanoparticles. Prior to in vivo evaluations, the anti-tumor effect of the DTX-loaded glycopolymeric nanoparticles was measured in vitro. Interestingly, compared to the free DTX group, the cell viability of 4T1 cells significantly decreased for all the nanoparticles **P-Fuc**/DTX, **P-SA**/DTX and **P-SF**/DTX within the concentration range of 0.5-32 mg/L (Figure 3C). The further calculated IC_{50} values (Figure 3D) of nanoparticles **P-Fuc**/DTX, **P-SA**/DTX, and **P-SF**/DTX against 4T1 cells were 25.2, 28.4 and 22.3 nM, respectively, much lower than that of free DTX (62.4 nM), demonstrating stronger anti-tumor activity of these DTX-loaded nanoparticles at cellular level. This can be attributed to the poor solubility of free DTX in water, hindering its actual functions inside cells, while the highly accelerated endocytosis rates of the DTX-loaded nanoparticles greatly strengthened their cellular toxicity. In addition, the similar IC_{50} values obtained from different glycopolymers can be explained by the fully cellular uptake of all the nanoparticles after extended incubation time.

In vivo tumor accumulation and long circulation. From the above in vitro investigations, glycopolymer **P-SF** demonstrated a faster endocytosis rate and stronger affinity to activated platelets compared to other glycopolymeric nanoparticles. Subsequently, the in vivo biodistribution of the **P-SF** was assessed using a 4T1 mouse model. As shown in Figure 4A, **P-SF**-Cy5 rapidly accumulated at the tumor site, exhibiting high fluorescent intensity as early as 0.2 h after injection and peaking at 8 h. Although the fluorescent intensity of **P-SF**-Cy5 gradually decreased after 12 h, strong signals persisted throughout the 24 h observation window. Meanwhile, under the same intensity scale, the fluorescence of free Cy5 was much lower and

almost invisible as compared to the **P-SF**-Cy5 group, which correlated well to the quantitative fluorescent analysis in Figure 4C (images see Figure S15). Moreover, after harvesting major organs and the tumor at 24 h, **P-SF**-Cy5 exhibited distinct fluorescent mapping at the kidney, lung and tumor sites (Figure 4B), while no evident accumulation of Cy5 anywhere, suggesting prolonged circulation time and highly enhanced tumor-targeting capability of **P-SF**-Cy5.

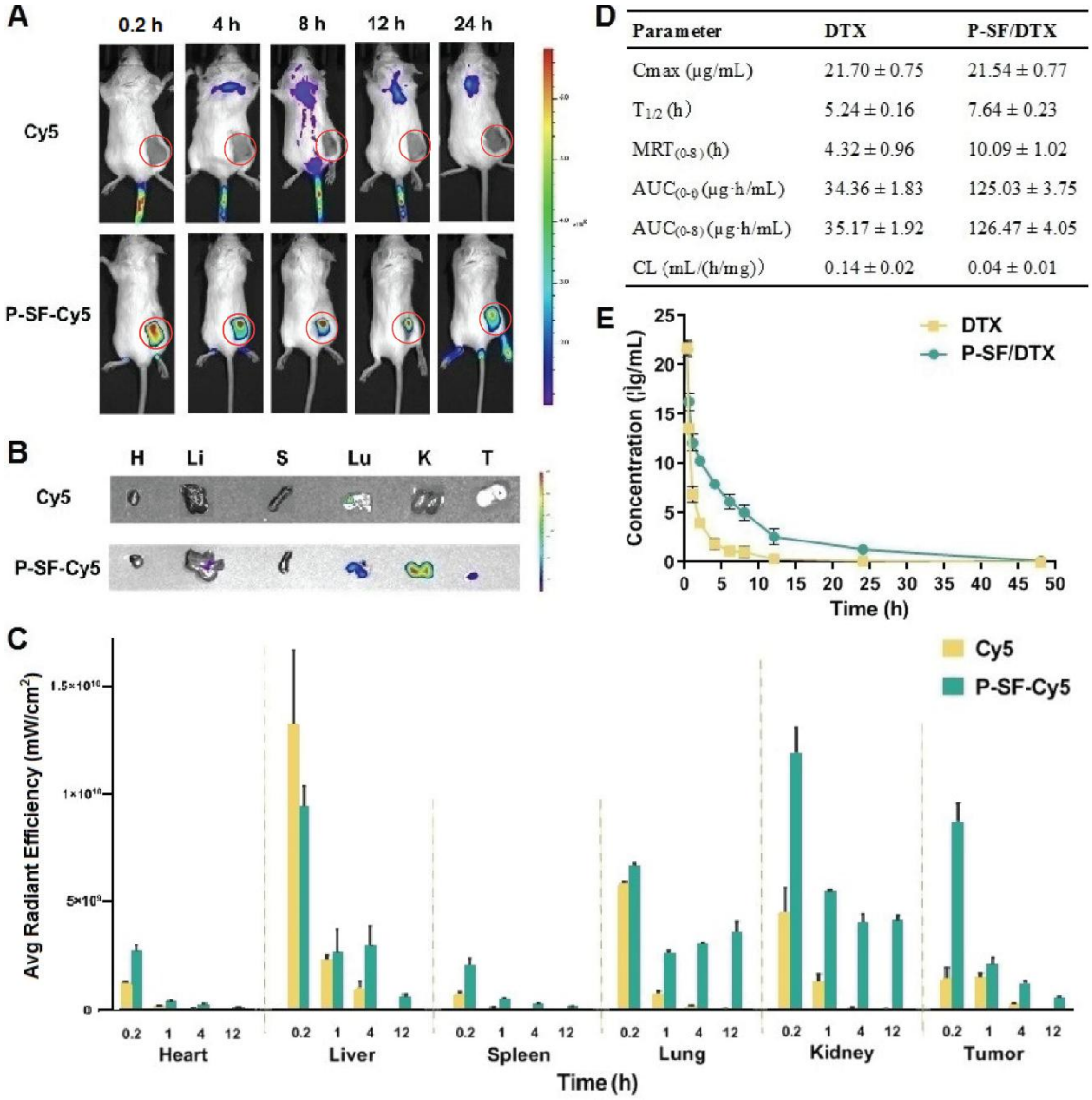

Parameter	DTX	P-SF/DTX
Cmax (μg/mL)	21.70 ± 0.75	21.54 ± 0.77
$T_{1/2}$ (h)	5.24 ± 0.16	7.64 ± 0.23
$MRT_{(0-8)}$ (h)	4.32 ± 0.96	10.09 ± 1.02
$AUC_{(0-t)}$ (μg·h/mL)	34.36 ± 1.83	125.03 ± 3.75
$AUC_{(0-8)}$ (μg·h/mL)	35.17 ± 1.92	126.47 ± 4.05
CL (mL/(h/mg))	0.14 ± 0.02	0.04 ± 0.01

Figure 4. Biodistribution of nanoparticles on the 4T1 primary tumor model: (A) in vivo fluorescence imaging of 4T1-bearing mice at different times after administration of different preparations (2 mg/kg Cy-5). The tumor sites are indicated with red circles.; (B) ex vivo fluorescence images of major organs and tumors at 24 h; (C) quantitative analysis of the

fluorescence intensities of major organs and tumors after the treatment of Cy-5 and **P-SF-**Cy5 for 0.2, 1, 4 and 12 h (n=5). (D) Pharmacokinetic parameters of DTX and **P-SF**/DTX. (E) The drug concentration–time curve of free DTX, **P-SF**/DTX (DTX-equivalent 5 mg/kg). Data are presented as mean ± SD (n=3).

Further quantitative analysis of sample accumulation in harvested tumors and organs revealed that as high as 21.0% of **P-SF**-Cy5 accumulated in the tumor for the initial 0.2 h, displaying significantly higher fluorescent intensity than Cy5. In contrast to the fast decrease of Cy5 signals across all organs within the following 12 h, the tumor accumulation rate of **P-SF**-Cy5 remained at 15.3% after 1 h, while maintaining substantial fluorescent intensities in tumors at 12 h (Figure 4C).

As a natural component in blood, platelets possess relatively long lifetime in the circulatory system. By adhering on platelets, the DTX-loaded nanoparticle **P-SF**/DTX may have the potential for extended circulation. To conduct the pharmacokinetics assay, free DTX or **P-SF**/DTX (DTX-equivalent as 5 mg/kg) was intravenously injected into BALB/c mice, and the whole blood were collected at predetermined time intervals. Based on the calculated pharmacokinetic parameters and the drug concentration-time curve in Figure 4D-E, **P-SF**/DTX had a significantly larger area under the curve $AUC_{0-\infty}$ (126.47 μg·h/mL) than DTX (35.17 μg·h/mL), and a notably prolonged $t_{1/2}$ (7.64 h) compared to free DTX (5.24 h). Additionally, the mean residence time ($MRT_{0-\infty}$) of **P-SF**/DTX was extended to 10.09 h, more than double that of free DTX (4.32 h).

In vivo anti-tumor and anti-metastasis efficacies. Following the promising in vitro and in vivo biodistribution results, a 4T1 tumor bearing-mouse model Figure 5A was used to evaluate the in vivo anti-tumor efficacy by intravenously administrating DTX-loaded nanoparticles. As shown in Figure 5B, free DTX had a certain inhibitory effect on tumor growth compared to the

rapidly growing tumor volume of the PBS group. However, the tumor volume resumed rapid growth after the injection ended. Meanwhile, the tumor suppression effect following the injection of nanoparticle **P-SF**/DTX was much better throughout the observation period, with the final tumor volume recorded as 231 mm^3, only 30% compared to that of PBS group, and 19% compared to the free DTX group.

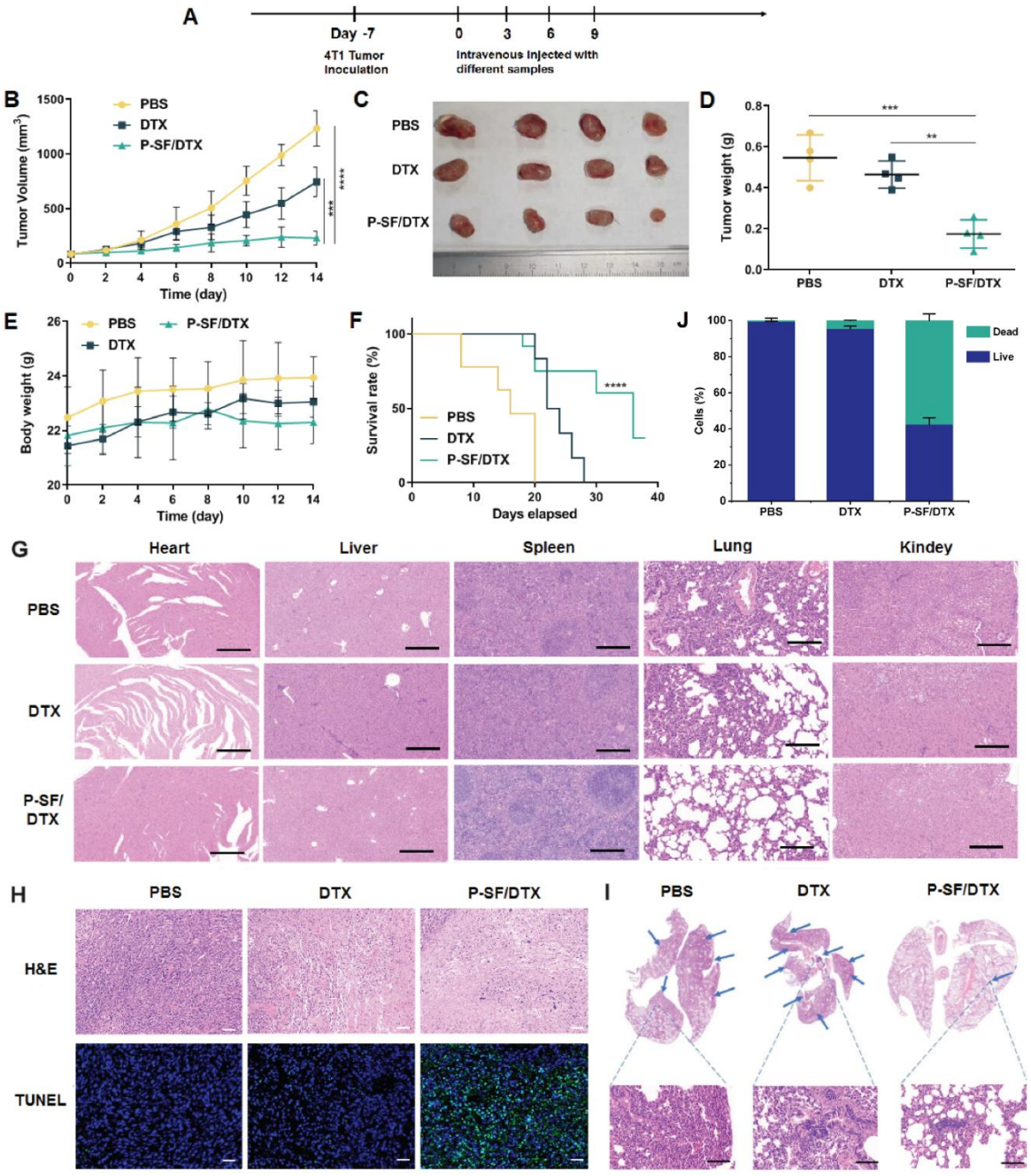

Figure 5. In vivo antitumor effect of drug-loaded nanoparticles: (A) treatment scheme of the samples; (B) tumor volume change of 4T1-bearing mice; (C) representative images of tumors after treatment and (D) tumor weight; (E) body weight change of tumor-bearing mice (n = 5). (F) Kaplan-Meier survival curves of 4T1-bearing mice (n = 6) after different treatments, Log-rank test determined statistical significance. (G) H&E and TUNEL-stained sections at tumor sites. Blue: nucleus; green: apoptosis cells. Scale bar = 100 μm. (H) H&E staining of major organs after treatment. Scale bar: 100 μm. (I) Anti-metastasis effect of glycopolymeric nanoparticles. H&E staining images of lungs. Scale bar = 100 μm. (J) Semi-quantitative analysis of the live and dead cells in the TUNEL images. ** $p < 0.01$, *** $p < 0.001$, and **** $p < 0.0001$.

The excised tumors were weighed and photographed after the mice were sacrificed on day 14, and the considerably lower tumor weight from **P-SF**/DTX verified its suppression effect for tumor growth (Figure 5C-D). Additionally, none of the treatments caused the mice body weight to decrease (Figure 5E), suggesting no obvious toxicity of DTX to mice at the current feeding dosage. The excellent anticancer activity of **P-SF**/DTX also significantly prolonged the mice survival time. As displayed in Figure 5F, compared to the median survival of 16 and 22 days for saline and DTX groups, respectively, the mice treated with **P-SF**/DTX achieved the longest median survival time of 36 days.

H&E staining of the tumor sections revealed increased necrosis following DTX or **P-SF**/DTX treatment, along with significantly reduced cell nuclei in Figure 5H, 5J. The TUNEL staining results indicated a higher percentage of apoptotic cells in the **P-SF**/DTX group, with almost no fluorescence seen in the PBS or free DTX group. Furthermore, in the collected major organ slices of mice (Figure 5G), significantly reduced vacuoleization in the heart muscle fibers was observed in the **P-SF**/DTX group compared to free DTX treatment, indicating lowered cardiotoxicity of DTX with targeted delivery by nanoparticle **P-SF**.

Metastasis is a critical stage in the progression of tumor deterioration. We have previously reported a series of monosaccharide- or disaccharide-grafted glycopolymers for anti-metastasis studies,[14, 35] including the hybrid co-polymerization of fucose and sialic acid. Subsequently, the anti-metastasis activity of the DTX-loaded nanoparticles was evaluated. As can be seen in Figure

5I, there were more lung nodules in the PBS and DTX groups, while almost none were found on the lung surfaces from the **P-SF**/DTX group. These findings confirmed the strong inhibitory effect of nanoparticle **P-SF** on lung metastasis, owing to its strong binding ability with activated platelets, which inhibited the adhesion between tumor cells and platelets before initiating the metastasis process.

CONCLUSION

Platelet-mediated drug delivery has recently emerged as an efficient strategy for cancer therapy, prevalently through membrane coating strategy. In the current study, we developed a new type of amphiphilic glycopolymer-based micellar nanoparticles for targeted delivery of anti-tumor drug DTX to tumors.[24-27] The glycopolymers grafted with both sialic acid and fucose segments exhibited high affinity for activated platelets. With the tumor-homing effect of the activated platelets, the drug-loaded micellar nanoparticles can be guided for facilitated transportation and enhanced accumulation at the tumor site. The in *vitro* experiments showed excellent biocompatibility of the glycopolymeric nanoparticles towards normal cells, selectively accelerated endocytosis rates into tumor cells, pH-responsive drug release behavior, and even higher cytotoxicity towards tumor cells compared to free DTX. Subsequent in *vivo* experiments revealed fast and enhanced accumulation of the DTX-loaded glycopolymeric nanoparticles in tumors, along with excellent anti-tumor property, prolonged survival time and reduced cardiotoxicity. Furthermore, the nanoparticles exhibited an anti-tumor lung metastasis effect, indicating excellent efficacy of the DTX-loaded glycopolymeric nanoparticles in treating local tumor and preventing metastasis. Upon delicate turning of carbohydrate segments in the

glycopolymers, the platelet-adhesion nanoparticles in this study offered a new approach for tumor-targeted drug delivery, suggesting a significant potential for future cancer therapy.

MATERIALS AND METHODS

Materials. Acrylic acid, hydrazine hydrate, methacrylic anhydride, glucose, fucose, sialic acid, aniline, hydroquinone, trisodium citrate and ammonium acetate buffer were purchased from Sinopharm Chemical Reagent Co., Ltd (Shanghai, China). 4-Cyanopentanoic acid dithiobenzoate, 2,2'-diazobis(2-methylpropionitrile) (AIBN), dodecylamine and docetaxel (DTX) were purchased from SAN Chemical Technology Co., Ltd (Shanghai, China). Thrombin and Cy5 were purchased from Meilun Biological Technology Co., Ltd (Dalian, China). RPMI1640 medium, Dulbecco's modified Eagle's medium (DMEM) and fetal bovine serum (FBS) were obtained from Gibco Life Technology Co., Ltd (Carlsbad, CA, USA).

Cell Lines and Animals. Embryonic mouse fibroblasts cells (NIH-3T3) and mouse breast cancer cells (4T1) were purchased from the Shanghai Institutes for Biological Sciences (SIBS, Shanghai, China). Female BALB/c mice (6-8 weeks) were purchased from Sibeifu Experimental Animal Company (Suzhou, China). All animal experiments were performed in accordance with the guidelines approved by Experimental Animals Administrative Committee of Jiangnan University (Wuxi, China).

Syntheses of the Glycopolymer Nanoparticles. The glycopolymers were synthesized by reversible addition-broken chain transfer polymerization (RAFT). Initially, the synthetic method for polymerizable monomers has been described in supporting information file. Thereafter, 1 mmol carbohydrate monomer was added into 1 mL DMF, followed by addition of 4-

cyanovalerate dithiobenzoate (13.9 mg, 0.05 mmol) as the chain transfer agent and 2,2'-diazobis(2-methylpropionitrile) (1.64 mg, 0.01 mmol) as the free radical initiator. The resulted mixture was kept stirring at 75 °C for 24 h under N_2 protection. *N*-dodecyl acrylamide was subsequently added, and the mixture was stirred for another 24 h. The crude product was purified by dialysis and freeze-dried to obtain the final glycopolymers.

Characterization of the Nanoparticles. The average molecular weight and the dispersion index of the glycopolymers were obtained by gel permeation chromatography (GPC) using Shodex OHPak SB-803HQ column, with 0.2 M NaCl as the mobile phase at rt and the flow rate set as 0.5 mL/min. The particle sizes of the nanoparticles were initially analyzed by a laser scattering particle analyzer (Malvern Instruments Co., Ltd., Zetasizer Nano ZS90, Worcestershire, UK), from the samples prepared as 1 mg/mL solution in deionized water. The nanoparticle morphologies were also observed by a transmission electron microscope (TEM, JEOL, JEM-100CXII, Japan) under 120 kV, where the samples were prepared by dissolving in deionized water and dropped onto the carbon-coated copper grids.

Drug Loading and Release. DTX (5 mg) solution in 5 mL $CHCl_3$ was added into 20 mL glycopolymer (20 mg) solution in deionized water under strong stirring, and the resulted mixture was stirred for 24 h. After complete evaporation of chloroform, the solution was centrifuged at a speed of 4000 rpm, with the solid part collected and freeze-dried. The glycopolymer nanoparticles loaded with DTX (20 mg) were dissolved in a dialysis bag with PBS (pH 5.5 or 7.4) at 37 °C, then 5 mL solution was taken from the dialysis system at predetermined time intervals, and then immediately replenished with 5 mL PBS. The drug loading and release efficiency was determined by a UV spectrophotometer (Thermo, vario micro cube, USA) at the wavelength of 229 nm.

In Vitro Cytotoxicity Assay. 3T3 and 4T1 cells were first added to a 96-well plate with the amount of 6×103 cells/well (100 μL) and incubated at 37 °C under 5% CO_2 with their corresponding mediums for 24 h. Then, drug-loaded glycopolymers of different concentrations (50-200 mg/L) were added to each well, and the culture process was extended for an additional 24 h. Thereafter, each well was treated with 0.5 mg/mL MTT solution and incubated for 4 h. The cytotoxicity of the glycopolymers was examined on a microplate reader at the wavelength of 570 nm. Each sample was performed with six replicates.

Adhesion of Platelets to Tumor Cells. Fresh blood was taken from BALB/c mice, with immediate anticoagulation by 10% (v/v) of 3.8% trisodium citrate, and left at rt for 30 min. After centrifugation at 200 g to remove the upper-layer serum, the lower part was centrifuged again at 1200 g, with the platelets collected as white pellets by aspirating the supernatant. The activated platelets were obtained by incubation the re-suspended platelets in PBS (pH 7.4) with thrombin (1 U/mL) at 37 °C for 30 min. For cell adhesion analysis, 3T3 and 4T1 cells were first digested with PBS and diluted to 10^5/mL cell suspension, 100 μL of which was added to a 6-well plate, followed by incubation at 37 °C under 5% CO_2 atmosphere for 4 h. Thereafter, 100 μL activated platelet suspension in PBS (pH 7.4) with the dilution to 10^8/mL was added. After incubation for 1 h, the adhesion status of the platelets to 3T3 or 4T1 was photographed under a microscope (Nikon, Japan).

Adhesion of Nanoparticles to Activated Platelets. 10^8 inactivated platelets were added to the confocal dish, leaving at 37 °C for 1 h to adhere to the plate. After activation, different glycopolymer nanoparticles were added and incubated at 37 °C for another 30 min. After washing the unconsolidated nanoparticles with PBS for 3 times, the bound platelets were observed by confocal laser scanning microscope (CLSM, Nikon, Japan). For further

quantification analysis, rhodamine B-tagged glycopolymers were used. After centrifugation, the platelets were resuspended in PBS (pH 7.4), and the mean fluorescence intensities were acquired by flow cytometry (Beckman Coulter, Inc., Cytomics FC 500, CA, US).

In Vitro inhibition of tumor cell adhesion. Platelets (100 μL, 1×10^8 /ml) solution in PBS were added to a 96-well plate and incubation at 37 °C for 2 h to bind the platelets to the bottom of the wells. After platelets activation by thrombin for 15 min and washing away the extra thrombin, 100 μL of 4T1 cell suspension (5×10^6 /ml) containing different samples (200 μg/mL) was added to each well and incubated at 37 °C for 30 min. Followed washing away the unbound cells, static observation was performed using a microscope. The cells were then re-suspended in PBS and the adhered 4T1 cells was detected by flow cytometry.

In vitro tumor cell migration test. The 4T1 cells was diluted to a concentration of 1×10^6/mL, with 100 uL of cell suspension added to the upper layer of the Transwell chamber. 600 μL serum free medium containing the samples was added to the well plates, and incubated at 37 °C under 5% CO_2 for 24 h. Thereafter, the culture medium of the upper layer of the chamber was aspirated and washed with PBS. The cells were fixed with 4% paraformaldehyde for 10 min and washed with PBS, followed by permeabilization with methanol for 20 min. After washing with PBS, the cells were stained with 0.1% crystalline violet for 2 h. After washing, the migration of 4T1 cells was observed and photographed under a microscope. The lower layer of crystal violet was washed with 33% acetic acid solution, and the UV absorption at 570 nm was measured. The cell migration rate was calculated using the following formula.

$$\text{Transwell migration} = \frac{OD_{Sample}}{OD_{Control}} \times 100\%$$

OD_{Sample} is the absorbance of the treated well; $OD_{Control}$ is the absorbance of cell wells with only serum-containing medium.

In Vitro Cellular Uptake Studies. 8×10^4 4T1 cells were seeded into 6-well plates and incubated at 37 °C under 5% CO_2 atmosphere for 18 h. Then the medium was replaced by **P-Fuc**, **P-SA** or **P-SF** solution, respectively. After incubation for 1 or 4 h, the unconsolidated nanoparticles were washed with PBS for 3 times, and the cells were stained with DAPI and observed by CLSM. Meanwhile, the impacts of platelets on cellular uptake was evaluated by pre-incubating the activated platelets with 4T1 cells for 30 min, followed by addition of the glycopolymer nanoparticles. Then, the same procedures of incubation, washing and staining were performed.

In Vivo Biodistribution. The tumor-bearing mice were injected with Cy-5 and **P-SF**-Cy5 (2 mg/kg equivalent Cy5) via tail veins, respectively, and in vivo imaging of small animals was performed at predetermined time intervals of 0.25, 4, 8, 12 and 24 h, respectively. After 24 h, the mice were sacrificed and the major organs of heart, liver, spleen, lung, kidney and tumor were taken for photographing and imaging by In Vivo Imaging System (IVIS, PerkinElmer, Inc., Lumina Series III, CA, US). For the quantitive fluoresence assay, the mice were sacrificed at 0.2, 1, 4, and 12 h after injection, with the major organs and tumors collected. Subsequently, the in vitro organs were imaged and the fluorescent intensity was quantified using IVIS system.

Pharmacokinetic Assay. BALB/c mice (n=3) were injected with DTX, **P-SF**/DTX (5 mg/kg equivalent DTX) through tail vein, respectively. 40 μL blood per mice was collected in heparin-treated tubes at predetermined time intervals of 0.25, 0.5, 1, 2, 4, 6, 8, 12, 24 and 48 h. The blood samples were then extracted with $CHCl_3$ to obtain plasma. The content of DTX in plasma was detected by HPLC (Shimadzu, LC-20A, Japan), and the pharmacokinetic parameters were calculated with Winnonlin (Pharsight, USA).

In Vivo Anti-tumor/Anti-metastasis Assessment and Survival Curve. BALB/c mice were selected for mouse subcutaneous tumor modeling. Each mice was inoculated with 1×10^6 4T1 cells subcutaneously, and injected with PBS, DTX, **P-SF**/DTX (5 mg/kg equivalent DTX) via tail vein one week later. A total of 4 injections were given every three days. The changes of tumor volume (V) and body weight were recorded every two days. After execution, the vital organs and the tumor were taken for H&E staining, meanwhile, tumors were taken for TUNEL staining. To evaluate the survival of the mice, 18 tumor 4T1-bearing mice were divided into 3 groups randomly, followed by the treatments of PBS, DTX, **P-SF**/DTX (5 mg/kg equivalent DTX). The survival rates of mice were analyzed by the Kaplan−Meier curve.

Statistical analysis. All results were given as means ± SD. To determine the statistical significance, comparison between the two groups was performed by one-way ANOVA tests. $P < 0.05$ (*), $P < 0.01$ (**), $P < 0.001$ (***), or $P < 0.0001$ (****) was considered statistically significant.

ASSOCIATED CONTENT

Supporting Information. The following Supporting Information is available free of charge.

Synthesis and characterization of the polymerizable monomers and glycopolymers, including ^{1}H NMR and FT-IR spectra and GPC; synthesis of fluorescent reagents-tagged compounds; establishment of the DTX standard curve by UV-Vis and HPLC methods; additional images of cellular uptake.

AUTHOR INFORMATION

Corresponding Authors

*Yan Zhang - *Key Laboratory of Carbohydrate Chemistry and Biotechnology, Ministry of Education, School of Pharmaceutical Sciences, Jiangnan University, Wuxi, 214122, P.R. China*;

orcid.org/0000-0003-2479-7555;

Email: zhangyanyz@jiangnan.edu.cn.

*Mihail Barboiu- *Institut Europeen des Membranes, Adaptive Supramolecular Nanosystems Group, University of Montpellier, ENSCM-CNRS, UMR5635, Place E. Bataillon CC047, 34095 Montpellier, France*

orcid.org/0000-0003-0042-9483;

Email: mihail-dumitru.barboiu@umontpellier.fr

*Jinghua Chen - *Key Laboratory of Carbohydrate Chemistry and Biotechnology, Ministry of Education, School of Pharmaceutical Sciences, Jiangnan University, Wuxi, 214122, P.R. China*;

orcid.org/0000-0001-8122-8450;

Email: chenjinghua@jiangnan.edu.cn

Funding Sources

This work was supported by National Key R&D Program of China [2021YFC2103100], National Natural Science Foundation of China [22008090], and Natural Science Foundation of Jiangsu Province [BK20180625].

Notes

The authors declare no competing financial interest.

REFERENCES

1. Wilhelm, S.; Tavares, A. J.; Dai, Q.; Ohta, S.; Audet, J.; Dvorak, H. F.; Chan, W. C. W., Analysis of nanoparticle delivery to tumours. *Nat. Rev. Mater.* **2016,** *1* (5), 16014.

2. Dutta, B.; Barick, K. C.; Hassan, P. A., Recent advances in active targeting of nanomaterials for anticancer drug delivery. *Adv. Colloid Interface Sci.* **2021,** *296*, 102509.

3. Ouyang, B.; Poon, W.; Zhang, Y.-N.; Lin, Z. P.; Kingston, B. R.; Tavares, A. J.; Zhang, Y.; Chen, J.; Valic, M. S.; Syed, A. M.; MacMillan, P.; Couture-Senécal, J.; Zheng, G.; Chan, W. C. W., The dose threshold for nanoparticle tumour delivery. *Nat. Mater.* **2020,** *19* (12), 1362-1371.

4. Attia, M. F.; Anton, N.; Wallyn, J.; Omran, Z.; Vandamme, T. F., An overview of active and passive targeting strategies to improve the nanocarriers efficiency to tumour sites. *J. Pharm. Pharmacol.* **2019,** *71* (8), 1185-1198.

5. Wang, W.; Zhao, B.; Zhang, Z.; Kikuchi, T.; Li, W.; Jantrawut, P.; Feng, F.; Liu, F.; Zhang, J., Natural polysaccharides and their derivatives targeting the tumor microenvironment: A review. *Int. J. Biol. Macromol.* **2024,** *268*, 131789.

6. Li, B.; Lu, F.; Wei, X.; Zhao, R., Fucoidan: Structure and Bioactivity. *Molecules* **2008,** *13* (8), 1671-1695.

7. Van Weelden, G.; Bobiński, M.; Okła, K.; Van Weelden, W. J.; Romano, A.; Pijnenborg, J. M. A., Fucoidan Structure and Activity in Relation to Anti-Cancer Mechanisms. *Mar. Drugs* **2019,** *17* (1), 32.

8. Pramudya, I.; Chung, H., Recent Progress of Glycopolymer Synthesis for Biomedical Applications. *Biomater. Sci.* **2019,** *7* (12), 4848-4872.

9. Miura, Y.; Hoshino, Y.; Seto, H., Glycopolymer Nanobiotechnology. *Chem. Rev.* **2016,** *116* (4), 1673-1692.

10. Miura, Y., Design and Synthesis of Well-defined Glycopolymers for the Control of Biological Functionalities. *Polym. J.* **2012,** *44* (7), 679-689.

11. Stenzel, M. H., Glycopolymers for Drug Delivery: Opportunities and Challenges. *Macromolecules* **2022,** *55* (12), 4867-4890.

12. Gerling-Driessen, U. I. M.; Hoffmann, M.; Schmidt, S.; Snyder, N. L.; Hartmann, L., Glycopolymers Against Pathogen Infection. *Chem. Soc. Rev.* **2023,** *52* (8), 2617-2642.

13. Sun, K.; Xu, M.; Zhou, K.; Nie, H.; Quan, J.; Zhu, L., Thermoresponsive Diblock Glycopolymer by RAFT Polymerization for Lectin Recognition. *Mater. Sci. Eng. C* **2016,** *68*, 172-176.

14. Cai, Z.; Teng, L.; Zhou, J.; Yan, Y.; Zhang, Y.; Lv, G.; Chen, J., Design and Synthesis of a Native Heparin Disaccharide Grafted Poly‐2‐aminoethyl Methacrylate Glycopolymer for Inhibition of Melanoma Cell Metastasis. *Int. J. Biol. Macromol.* **2019,** *126*, 612-619.

15. Yilmaz, G.; Becer, C. R., Glycopolymer Code: Programming Synthetic Macromolecules for Biological Targeting. *Macromol. Chem. Phys.* **2020,** *221* (7), 2000006.

16. Tyagi, T.; Jain, K.; Gu, S. X.; Qiu, M.; Gu, V. W.; Melchinger, H.; Rinder, H.; Martin, K. A.; Gardiner, E. E.; Lee, A. I.; Tang, W. H.; Hwa, J., A Guide to Molecular and Functional Investigations of Platelets to Bridge Basic and Clinical Sciences. *Nat. Cardiovasc. Res.* **2022,** *1* (3), 223-237.

17. Lu, Y.; Hu, Q.; Jiang, C.; Gu, Z., Platelet for Drug Delivery. *Curr. Opin. Biotechnol.* **2019,** *58*, 81-91.

18. In ‘t Veld, S. G. J. G.; Wurdinger, T., Tumor-educated Platelets. *Blood* **2019,** *133* (22), 2359-2364.

19. Wang, Y.; Li, Z.; Mo, F.; Gu, Z.; Hu, Q., Engineered Platelets: Advocates for Tumor

Immunotherapy. *Nano Today* **2021,** *40*, 101281.

20. Wang, S.; Duan, Y.; Zhang, Q.; Komarla, A.; Gong, H.; Gao, W.; Zhang, L., Drug Targeting via Platelet Membrane-Coated Nanoparticles. *Small Struct.* **2020,** *1* (1), 2000018.

21. Hu, Q.; Sun, W.; Qian, C.; Wang, C.; Bomba, H. N.; Gu, Z., Anticancer Platelet-Mimicking Nanovehicles. *Adv. Mater.* **2015,** *27* (44), 7043-7050.

22. Crunkhorn, S., Engineered Platelets Deliver Immunotherapy. *Nat. Rev. Drug Discov.* **2017,** *16* (3), 166-166.

23. Zhang, Y.; Sun, Y.; Dong, X.; Wang, Q.-S.; Zhu, D.; Mei, L.; Yan, H.; Lv, F., A Platelet Intelligent Vehicle with Navigation for Cancer Photothermal-Chemotherapy. *ACS Nano* **2022,** *16* (4), 6359-6371.

24. Li, H.; Wang, Z., Disrupting Tumour Vasculature and Recruitment of a PDL1-loaded Platelets Control Tumour Metastasis. *Nat. Commun.* **2021,** *12* (1), 2773.

25. Song, Y.; Huang, Z.; Liu, X.; Pang, Z.; Chen, J.; Yang, H.; Zhang, N.; Cao, Z.; Liu, M.; Cao, J.; Li, C.; Yang, X.; Gong, H.; Qian, J.; Ge, J., Platelet Membrane-coated Nanoparticle-mediated Targeting Delivery of Rapamycin Blocks Atherosclerotic Plaque Development and Stabilizes Plaque in Apolipoprotein E-deficient (ApoE−/−) mice. *Nanomedicine: NBM* **2019,** *15* (1), 13-24.

26. Wang, S.; Wang, R.; Meng, N.; Guo, H.; Wu, S.; Wang, X.; Li, J.; Wang, H.; Jiang, K.; Xie, C.; Liu, Y.; Wang, H.; Lu, W., Platelet Membrane-functionalized Nanoparticles with Improved Targeting Ability and Lower Hemorrhagic Risk for Thrombolysis Therapy. *J. Control. Release* **2020,** *328*, 78-86.

27. Wei, X.; Ying, M.; Dehaini, D.; Su, Y.; Kroll, A. V.; Zhou, J.; Gao, W.; Fang, R. H.; Chien, S.; Zhang, L., Nanoparticle Functionalization with Platelet Membrane Enables Multifactored

Biological Targeting and Detection of Atherosclerosis. *ACS Nano* **2018,** *12* (1), 109-116.

28. Guo, R.; Deng, M.; He, X.; Li, M.; Li, J.; He, P.; Liu, H.; Li, M.; Zhang, Z.; He, Q., Fucoidan-Functionalized Activated Platelet-Hitchhiking Micelles Simultaneously Track Tumor Cells and Remodel the Immunosuppressive Microenvironment for Efficient Metastatic Cancer Treatment. *Acta Pharm. Sin. B* **2022,** *12* (1), 467-482.

29. Li, B.; Juenet, M.; Aid-Launais, R.; Maire, M.; Ollivier, V.; Letourneur, D.; Chauvierre, C., Development of Polymer Microcapsules Functionalized with Fucoidan to Target P-Selectin Overexpressed in Cardiovascular Diseases. *Adv. Healthc. Mater.* **2017,** *6* (4), 1601200.

30. Juenet, M.; Aid-Launais, R.; Li, B.; Berger, A.; Aerts, J.; Ollivier, V.; Nicoletti, A.; Letourneur, D.; Chauvierre, C., Thrombolytic Therapy based on Fucoidan-functionalized Polymer Nanoparticles Targeting P-selectin. *Biomaterials* **2018,** *156*, 204-216.

31. Li, S.; Lu, Z.; Wu, S.; Chu, T.; Li, B.; Qi, F.; Zhao, Y.; Nie, G., The dynamic role of platelets in cancer progression and their therapeutic implications. *Nat. Rev. Cancer* **2024,** *24* (1), 72-87.

32. Tylawsky, D. E.; Kiguchi, H.; Vaynshteyn, J.; Gerwin, J.; Shah, J.; Islam, T.; Boyer, J. A.; Boué, D. R.; Snuderl, M.; Greenblatt, M. B.; Shamay, Y.; Raju, G. P.; Heller, D. A., P-selectin-targeted nanocarriers induce active crossing of the blood–brain barrier via caveolin-1-dependent transcytosis. *Nat. Mater.* **2023,** *22* (3), 391-399.

33. Jafari, M.; Sriram, V.; Xu, Z.; Harris, G. M.; Lee, J.-Y., Fucoidan-Doxorubicin Nanoparticles Targeting P-Selectin for Effective Breast Cancer Therapy. *Carbohydr. Polym.* **2020,** *249*, 116837.

34. Bachelet, L.; Bertholon, I.; Lavigne, D.; Vassy, R.; Jandrot-Perrus, M.; Chaubet, F.; Letourneur, D., Affinity of low molecular weight fucoidan for P-selectin triggers its binding to

activated human platelets. *Biochim. Biophys. Acta, Gen. Subj.* **2009,** *1790* (2), 141-146.

35. Cai, Z.; Yan, Y.; Zhou, J.; Yang, Y.; Zhang, Y.; Chen, J., Multifunctionalized Brush-Like Glycopolymers with High Affinity to P-Selectin and Antitumor Metastasis Activity. *Biomacromolecules* **2021,** *22* (3), 1177-1185.

36. Bernard, J.; Hao, X.; Davis, T. P.; Barner-Kowollik, C.; Stenzel, M. H., Synthesis of Various Glycopolymer Architectures via RAFT Polymerization: From Block Copolymers to Stars. *Biomacromolecules* **2006,** *7* (1), 232-238.

37. Otto, G., Selectins Block T Cells in SLE. *Nat. Rev. Rheumatol.* **2021,** *17* (9), 510-510.

38. Tinoco, R.; Otero, D. C.; Takahashi, A. A.; Bradley, L. M., PSGL-1: A New Player in the Immune Checkpoint Landscape. *Trends Immunol.* **2017,** *38* (5), 323-335.

39. Fang, H.; Chen, L.; Zeng, L.; Yang, Z.; Zhang, J., Stability, Stimuli-Responsiveness, and Versatile Sorption Properties of a Dynamic Covalent Acylhydrazone Gel. *Global Chall.* **2019,** *3* (2), 1800073.

40. Zhang, Y.; Barboiu, M., Constitutional Dynamic Materials—Toward Natural Selection of Function. *Chem. Rev.* **2016,** *116* (3), 809-834.

41. Raju Kutcherlapati, S. N.; Yeole, N.; Gadi, M. R.; Perali, R. S.; Jana, T., RAFT Mediated One-pot Synthesis of Glycopolymer Particles with Tunable Core–Shell Morphology. *Polym. Chem.* **2017,** *8* (8), 1371-1380.

42. Tanaka, J.; Archer, N. E.; Grant, M. J.; You, W., Reversible-Addition Fragmentation Chain Transfer Step-Growth Polymerization. *J. Am. Chem. Soc.* **2021,** *143* (39), 15918-15923.

43. Casey, J. R.; Grinstein, S.; Orlowski, J., Sensors and regulators of intracellular pH. *Nat. Rev. Mol. Cell Biol.* **2010,** *11* (1), 50-61.

44. Liang, K.; Richardson, J. J.; Ejima, H.; Such, G. K.; Cui, J.; Caruso, F., Peptide-Tunable

Drug Cytotoxicity via One-Step Assembled Polymer Nanoparticles. *Adv. Mater.* **2014,** *26* (15), 2398-2402.

45. Cui, J.; Yan, Y.; Wang, Y.; Caruso, F., Templated Assembly of pH-Labile Polymer-Drug Particles for Intracellular Drug Delivery. *Adv. Funct. Mater.* **2012,** *22* (22), 4718-4723.

46. Anvari, S.; Osei, E.; Maftoon, N., Interactions of Platelets with Circulating Tumor Cells Contribute to Cancer Metastasis. *Sci. Rep.* **2021,** *11* (1), 15477.

TOC Graphic

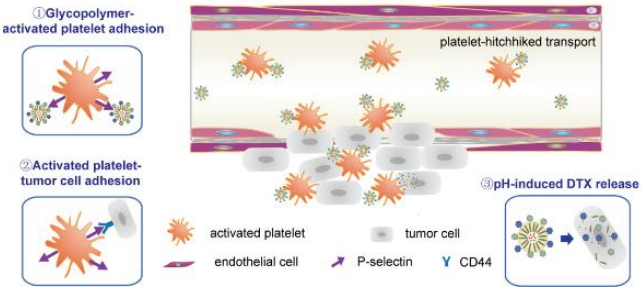
①Glycopolymer-activated platelet adhesion
platelet-hitchhiked transport
②Activated platelet-tumor cell adhesion
③pH-induced DTX release
activated platelet
tumor cell
endothelial cell
P-selectin
CD44